

Is the X-ray spectrum of the Seyfert 2 galaxy NGC5252 intrinsically flat ?

M. Cappi¹, T. Mihara¹, M. Matsuoka¹, W. Brinkmann²,
M. A. Prieto², G.G.C. Palumbo^{3,4}

¹ The Institute of Physical and Chemical Research (RIKEN), 2-1, Hirosawa, Wako, Saitama 351-01, Japan

² Max-Planck-Institut für extraterrestrische Physik, D-85748 Garching bei München, F.R.G.

³ Dipartimento di Astronomia, Università di Bologna, Via Zamboni 33, I-40126 Bologna, Italy

⁴ Istituto Te.S.R.E., CNR, Via Gobetti 101, I-40129, Bologna, Italy

Accepted for publication in the Astrophysical Journal (Main Journal).

Send correspondence to:

Massimo Cappi

The Institute of Physical and Chemical Research (RIKEN)

Hirosawa 2-1, Wako-shi,

Saitama 351-01, JAPAN

Tel:+81-48-462-1111 ext.3221

Fax:+81-48-462-4640

ABSTRACT

The first X-ray observation of the Seyfert 2 galaxy NGC5252 is reported. ASCA collected ~ 4000 photons/detector enough to perform an accurate spectral analysis of this source. The luminosity of NGC5252 is $L_X(0.7-10 \text{ keV}) \simeq 2.6 \times 10^{43} \text{ erg s}^{-1}$, typical of a Seyfert 1 galaxy. A simple description of the spectrum with a single power law is ruled out by the SIS data which shows a strong soft excess at $E \lesssim 1.2 \text{ keV}$. The spectrum is best fitted by models assuming either partial covering of the central source or scattering of the X-ray continuum. The best-fit partial covering model results in a flat ($\Gamma \simeq 1.45 \pm 0.2$) power law continuum emitted by a source almost completely covered (at $\sim 94-97\%$) by neutral matter ($N_H \simeq (4.3 \pm 0.6) \times 10^{22} \text{ cm}^{-2}$). The detected iron line is remarkably weaker (EW $\sim 90 \pm 60 \text{ eV}$) than normally found from Seyfert 2 galaxies. In an effort to interpret the observed flat spectrum with an intrinsically steep power law as predicted by unified models, we also included in the models neutral reflection, ionized absorption (warm absorber), and non-uniform cold absorption (dual-absorber). We find that the observed flat continuum **and** weakness of the iron line poses a problem for neutral reflection models, whatever the assumed geometry is. The use of an ionized absorber (scattering + warm-absorber model) instead of a neutral absorber seems not justified with the present data. The “dual-absorber” model, representing nonuniform (density) absorption along the line of sight, may provide an alternative explanation for the flatness of the spectrum, with no constraints on the Fe K emission line. Another plausible interpretation of the present data is that the X-ray spectrum of NGC5252 is truly intrinsically flat. Its strong similarities with the well-known Seyfert 1.5 NGC4151 are briefly discussed.

Key-words: galaxies: individual (NGC5252) - galaxies: Seyfert - X-rays: galaxies

1 Introduction

The discovery of broad emission lines in the polarized optical spectra of several Seyfert 2 galaxies (Antonucci & Miller 1985, Miller & Goodrich 1990, Tran et al. 1992) has provided the basis for a unified model of Seyfert galaxies in which the main discriminating parameter between Seyfert 1 and Seyfert 2 nuclei is the inclination to our line of sight of an obscuring torus surrounding the central source (see Antonucci 1993 for a review). In this scheme, Seyfert 1 galaxies are active nuclei observed nearly perpendicularly to the torus plane (unabsorbed) whereas Seyfert 2 galaxies represent those seen through the torus (absorbed). Further support of this scenario has come from GINGA X-ray observations which revealed the strongly absorbed spectra of some Seyfert 2 galaxies (Koyama et al. 1989, Awaki et al. 1991).

NGC5252 is an S0 galaxy at a redshift of $z \simeq 0.0234$. Its optical size is $\sim 1.4 \times 0.9$ arcmin, with the major axis being at a position angle $PA \sim 15^\circ$, and the absolute visual magnitude is $M_v = -21.4$ (Unger et al 1987). NGC5252 harbours a Seyfert 2 nucleus which illuminates a perfectly defined biconical structure of ionized gas extending up to 35 kpc from the nucleus (Tadhunter & Tsvetanov 1989). This is one of the largest extended ionized gas regions among nearby AGN. The axis of the bicone lies roughly at $PA \simeq 166^\circ$, close to the main axis of the 20 cm radio structure ($\simeq 172^\circ$). VLA HI observations of this galaxy revealed the existence of neutral gas located just outside the bicone of ionized gas. These findings provided unambiguous proof of the anisotropy of the radiation field in this galaxy (Prieto & Freudling 1993). Additional radio observations have detected weak, narrow extended features aligned with the larger scale optical ionization cones which further support the existence of collimation effects in NGC5252 (Wilson & Tsvetanov 1994).

Because of its favourable orientation with respect to the observer, NGC5252 is an ideal target for studying the collimation mechanism responsible for the observed anisotropy. Combined near IR and optical imaging have revealed the presence of a band of material across the nucleus and perpendicular to the bi-cone of ionized gas (Kotilainen & Prieto 1994). The band shows a gradually increasing extinction towards the center of the galaxy; a lower limit to the extinction of 6 mag is estimated.

Near IR spectroscopy of HeI $1.083 \mu\text{m}$ by Ruiz, Rieke & Schmidt (1994) shows

indeed a broad HeI component with FWHM $\sim 1050 \text{ km s}^{-1}$ thus revealing the typical signature of a Seyfert 1 nucleus. Polarization studies aimed at discovering the nature of the obscured nucleus via the nuclear light scattered by the surrounding material are not yet conclusive. Optical spectropolarimetry of the galactic nucleus indicates a $(11 \pm 11)\%$ polarization (Kay 1994). Given the strong (larger than 90%) stellar contribution to the nuclear optical light in this Seyfert 2 galaxy, polarization dilution by stellar light could be significant (Kay 1994; Kotilainen & Prieto 1994); alternatively, scattered light could also suffer extinction.

At the opposite extreme of the electromagnetic spectrum, broad-band X-ray data can provide crucial information on the hidden source because photons of a few keV may pass through the nuclear intervening material. It should be noted that since NGC5252 is an early-type galaxy, the contribution from star formation activity to the X-ray emission is expected to be minor. Indeed, deep H α imaging (Prieto & Freudling, in preparation) shows no trace of ionized gas outside the $[\text{OIII}]_{5007\text{\AA}}$ ionized bi-cone reported by Tadhunter & Tsvetanov (1989); most of this gas extends out of the galaxy plane. NGC5252 was not detected in the ROSAT all-sky survey. Based on these general considerations, we investigated the X-ray properties of NGC5252 with the ASCA observatory. To our knowledge, there is no report of any X-ray detection from previous missions. During the ASCA observations, enough photons were collected (section 2) to allow a detailed and accurate spectral analysis (section 3). This analysis is discussed in the light of recent observations of Seyfert galaxies and theoretical models (section 4). Our main results are summarized in section 5.

2 ASCA data reduction

ASCA observed NGC5252 between January 28 and January 31, 1994 with the Gas Imaging Spectrometer (GIS) for a total effective exposure time of about 70500 s and with the Solid-state Imaging Spectrometer (SIS) for about 65000 s. The SIS was operating in 1 or 2 CCD mode and all the data were collected in FAINT mode. DFE and echo corrections have been applied to the data (Otani & Dotani 1994). Good observational intervals were selected by applying the data selection criteria shown in Table 1.

Source counts were collected from a circle centered on the source of 4 arcmin radius for the GIS and 2.5 arcmin for the SIS. Background spectra were obtained using similar areas inside the Field of View (FOV) from uncontaminated regions. We checked for differences between different extraction regions for the source and the background but did not find any significant variations in the spectral results. In the GIS FOV, we detected elongated spurious emission in the direction north-west of NGC5252. This emission occurs in the direction of the ionized cones but we can exclude the possibility that it is related to NGC5252 because of the high separation (~ 10 arcmin) between the two. It is more likely associated with the bright SB galaxy MCG-01-35-024 whose position is coincident with the emitting region to within ~ 2 arcmin. We emphasize that the use of blank sky backgrounds for the GIS and SIS yielded spectral results within the errors reported in the following spectral analysis.

Relevant data for the NGC5252 observation are summarized in Table 2. Data preparation and analysis has been done using version 1.0h of the XSELECT package; spectral analysis has been performed using version 8.5 of the XSPEC program (Arnaud et al. 1991).

3 Spectral analysis

Source plus background light curves were computed in different energy bands: in the broad (0.4-10 keV), the soft (0.4-2 keV) and the hard (2-10 keV) energy bands. None of these lightcurves indicated significant variability; statistical χ^2 -tests against constancy give a probability $> 15\%$ in every case, i.e., consistent with constant source flux.

Therefore, we accumulated spectra from the photons collected in the total ~ 70 ks observation for the spectral analysis. The pulse height spectra were binned in such a way that there were at least 30 and 20 counts/bin for the GIS and SIS detectors and the corresponding energy bands were limited to 0.7-10 keV and 0.4-10 keV, respectively. We used the detector response matrices gisv3.1.rmf (GIS, released in March 1994) and rsp1.1.alpha (SIS, released in June 1994) and constructed the effective area at the source position with the program jbl darf-0.5a (released in January 1994).

3.1 Single power law fits

A single absorbed power law model was first fitted to the data with the effective hydrogen column density (N_{H}) left free to vary. The resulting best-fit parameters are given in Table 3. This simple model yielded an acceptable description of the GIS data in the 0.7-10 keV band with $\chi_{red}^2/\text{d.o.f.} \simeq 1.03/267$ but gives an unacceptable fit to the SIS data in the 0.4-10 keV band, with $\chi_{red}^2/\text{d.o.f.} \simeq 1.38/315$. The corresponding SIS spectrum is shown in Figure 1. The residuals of the SIS spectrum clearly indicate the presence of strong soft ($E \lesssim 1.2$ keV) X-ray emission in excess to the extrapolation of the higher energy continuum. It should be pointed out that the discrepancies between the GIS and SIS results (Table 3) are strongly reduced when the soft excess is explicitly fitted in the SIS spectrum as shown in the following sections. In all fits, the best-fit value of N_{H} is at least 2 orders of magnitude higher than the galactic absorption $N_{\text{Hgal}} \simeq 1.97 \times 10^{20}$ cm^{-2} (Dickey & Lockman 1990), suggesting strong intrinsic absorption.

It should be emphasized that, for completeness, an absorption component with $N_{\text{H}} = N_{\text{Hgal}}$ was also added to each model tested below in order to account for the absorption in our own galaxy. Because of its low value, however, the Galactic column is effective only at energies $E \lesssim 0.4$ keV.

3.2 Soft excess

3.2.1 Thermal soft-emission models

In a first attempt to model the soft X-ray excess, the broad-band pulse height spectrum was fitted with the following two-component models: (a) black body + absorption \times power law, (b) bremsstrahlung + absorption \times power law and (c) Raymond Smith + absorption \times power law, with the absorption applied to the power law free to vary in all models.

In model (a), the black body emission component could mimic the high energy tail of the spectrum emitted by an accretion disk. In models (b) and (c), it is assumed that the soft X-ray emission is produced by a thermal thin and hot gas associated with the host galaxy. In all three models, the hard power law is thought to be related to the nucleus itself. With all parameters free to vary, these models yielded acceptable fits to

the SIS data with $\chi_{red}^2/\text{d.o.f.} \sim 0.93\text{-}1.1/311$. Our results are reported in Table 4. All these models yielded similar values of N_{H} .

Fitting with model (a) gave $L_{\text{X}}(0.1\text{-}2.0 \text{ keV}) \simeq 3.9 \times 10^{41} \text{ erg s}^{-1}$ and a black body temperature of $T \simeq 2 \times 10^6 \text{ K}$. From these values, we deduce a characteristic dimension of the emitting region of $r \simeq 3 \times 10^9 \text{ cm}$ which is 2 orders of magnitude smaller than the Schwarzschild radius for a $10^6 M_{\odot}$ black hole. Therefore, a black-body + power law model does not provide a physically meaningful description of the data.

Thermal bremsstrahlung (model b) with a characteristic temperature $\sim 0.8 \text{ keV}$ together with a hard power law with $\Gamma \simeq 1.3 \pm 0.2$ provides a possible description of the data. However, this interpretation is inconsistent with the lack of soft emission lines in the ASCA spectrum which are expected to be emitted by a hot ($T \sim 10^7 \text{ K}$) plasma. The same problem is faced by a Raymond-Smith model (model c; Raymond & Smith 1977). In this case, metal abundances below ~ 0.01 solar are needed for acceptable fits, as reported in Table 4. These results, together with general arguments concerning the host galaxy (see section 4.1), make the hypothesis of a thermal origin for the soft-excess unlikely in the case of NGC5252.

3.2.2 Partial covering model

The observed SIS spectrum was then fitted with a partial covering model (Holt et al. 1980). This model consists of a power law continuum obscured by cold uniform matter with column density N_{H} , which covers a fraction C_{F} of the source. The model has 4 free parameters, namely the normalization, the photon index, the covering fraction and the column density. In physical terms, the absorbing material might be identified with thick and cold clouds distributed along the line of sight, covering only part of the central source.

As illustrated by the unfolded spectrum in Figure 2, this model provides a good description of the SIS (0.4-10 keV) spectrum with $\chi_{red}^2/\text{d.o.f.} \simeq 0.95/315$. The best-fit parameters are reported in Table 5a. Confidence contours for the photon index versus column density and for the covering fraction versus column density are shown in Figure 3. The best-fit parameters show that the SIS spectrum of NGC5252 is consistent with a flat ($\Gamma \simeq 1.45 \pm 0.2$) underlying power-law viewed through an absorber with column

density $N_{\text{H}} \simeq (4.3 \pm 0.6) \times 10^{22} \text{ cm}^{-2}$ which covers $\sim 96 \%$ of the primary source. The absorption corrected flux between 0.4-10 keV is $11.7 \times 10^{-12} \text{ erg cm}^{-2} \text{ s}^{-1}$. We emphasize that the reported errors correspond to 90% confidence limits for 3 interesting parameters and are, therefore, very conservative limits (Lampton et al. 1976).

The derived N_{H} value is equivalent to $A_{\text{v}} \sim 20 \text{ mag}$, for a standard gas to dust ratio, and thus is consistent with the large extinction towards the central source predicted from the IR-optical data (Kotilainen & Prieto 1994).

It should be pointed out that with the partial covering model the shape of the power-law in the SIS is consistent with the results obtained from the GIS instrument with a single power law model (section 3.1). Fitting the GIS data with a partial covering model, one obtains best-fit parameters which agree with the SIS results within $\sim 3\%$.

3.2.3 Scattering model

Another model which could describe the soft excess is a scattering model. Numerically equivalent to the partial covering model, it consists of the sum of 2 power laws having the same photon index but different absorptions and normalizations. One power law is absorbed by the Galactic column density only and the other is absorbed by a high intrinsic column density (a free parameter during the fit procedure). In this model the “non-absorbed” and absorbed power laws are related to the presence of scattering and obscuring matter, respectively. This interpretation is supported by unified models of AGN which predict that the direct continuum of Seyfert 2 galaxies is strongly obscured by a thick torus (Ghisellini, Haardt & Matt 1994) whereas part of the nuclear emission is scattered by free electrons surrounding the BLR (Antonucci & Miller 1985, Awaki et al. 1991).

As reported in Table 5b, the scattering model yields a good description of the data with $\chi_{red}^2/\text{d.o.f.} \simeq 0.95/312$, the best-fit parameters being again a flat power law with $\Gamma \simeq 1.46 \pm 0.2$, intrinsic absorption $N_{\text{H}} \simeq (4.4 \pm 0.6) \times 10^{22} \text{ cm}^{-2}$ ($\sim N_{\text{H}}$ partial covering), and a fraction of $\simeq 4\text{-}5\%$ of the continuum scattered into the observer’s line of sight.

3.3 Flat spectrum

On one side, *HEAO-1 A2* (Weaver, Arnaud & Mushotsky 1995) and *Ginga* (Nandra & Pounds 1994) results have shown that the *observed* canonical photon index $\Gamma_{2-18keV} \sim 1.7 - 1.8$ of Seyfert 1 galaxies can be interpreted as the sum of a steep *intrinsic* power law with $\Gamma_{2-18keV} \sim 1.8 - 2.1$ and a reflection component (e.g., Lightman & White 1988). On the other side, we still don't know very much about Seyfert 2 galaxies, as they are generally more absorbed and only few of them have high S/N X-ray spectra. Seyfert unification models (e.g., Antonucci 1993) predict the same average *intrinsic* photon index for Seyfert 1 and Seyfert 2 galaxies, but there is increasing evidence that the *observed* photon indices of several Seyfert 2 galaxies are flat with $\Gamma_{2-10keV} \sim 1.4 \pm 0.2$ (Awaki et al. 1991, Kunieda et al. 1994). Whether the *intrinsic* photon index of these is flat or not is an important question that directly impacts Seyfert unification models.

We have shown that all the models applied to NGC5252 require a flat power law. In light of the above considerations, it is therefore tempting to use more complex models to search for a global description of the spectrum with an intrinsically steep power law, as predicted by unified models. Therefore, in the following sections, we will focus on models involving (a) reflection by thick material, (b) absorption by ionized matter, and (c) line of sight obscuration. These models will be used together with the partial covering model (a and c) or scattering model (b). It should be borne in mind that though they imply different physical interpretations, the partial covering and scattering model cannot be distinguished with the present data (section 4.1) and would, therefore, give equivalent results if interchanged.

3.3.1 Reflection component and composite models

We first considered the possibility of explaining the apparently flat spectrum of NGC5252 with the presence of a reflection component. The existence of cold gas responsible for radiation reprocessing near the center of AGN is suggested by the strong UV emission in many observed AGN and is supported by theoretical considerations (Guilbert & Rees 1988). It is well established that the presence of this reflecting matter can strongly modify the observed X-ray spectrum. In particular, it could flatten the observed continuum (Lightman & White 1988) and provide an excellent explanation for at least part, if not

all, of the iron emission line intensity.

The reflection model used in the present analysis is the general case of neutral reflection from a slab of optically thick matter with $\tau_T \gg 1$ proposed by Lightman and White (1988), with opacities taken from Morrison and McCammon (1983). The spectrum is calculated integrating over all viewing angles and assuming isotropic emission from the source. The model used is the “plreff” reflection model available in the XSPEC fitting package (Arnaud et al. 1991). This model requires a total of 5 parameters, namely the photon index (Γ_{int}) and normalization (A_{pl}) of the primary power law, the normalization of the reflected component (A_{refl}), the slab inclination (i) and the fraction of the solid angle subtended by the slab ($\Omega/2\pi$). The latter parameter ($\Omega/2\pi$) has been fixed to 1 because it is redundant with A_{refl} in the fitting procedure. The inclination i was fixed to 0 (slab assumed face-on) because the shape of the reflected continuum is only a weak function of the inclination. In its simplest form, the one used here, this model is completely determined by only 3 (free) parameters (Γ_{int} , A_{pl} and A_{refl}). By examining the ratio $R \equiv A_{refl}/A_{pl}$, we can then make inferences about these parameters. For example, a value of $R \sim 1$ is consistent with an isotropic source covered by $\Omega/2\pi \sim 1$. A value of $R > 2$ cannot be explained with only an increase in $\Omega/2\pi$, but requires a time lag effect or/and anisotropic emission from the source.

This model was combined together with the partial covering model (section 3.2.2), yielding a total of 5 free parameters (one additional one if compared to the single partial covering model). The photon index was left free to vary. The resulting best-fit parameters are reported in Table 6 and the best-fit model is shown in Figure 4. The inclusion of a reflection component improves the fit by $\Delta\chi^2 \sim 6$, which is significant at more than 95% significance level for the addition of one free parameter. The resulting amount of reflection is $R \simeq 7.2_{-5}^{+7.6}$ and the photon index is $\Gamma \simeq 1.91 \pm 0.33$. The errors quoted here and below in this work represent 90% confidence intervals for 1 interesting parameter ($\Delta\chi^2 = 2.701$, Avni 1976). It is clear from these values and from Figure 4 that a very strong reflection component is necessary if one wants to model the observed flat shape at energies $4 < E < 10$ keV with an underlying steep power law.

The data are therefore consistent with an intrinsically steep ($\Gamma \sim 1.9$) power law provided there is a very strong ($R \sim 7$) reflection component. However, as will be

discussed later (section 4.2), the presence of such a strong reflection is unlikely, though not ruled out, in NGC5252 because it predicts a stronger than observed iron $K\alpha$ line (section 3.4).

3.3.2 Warm absorber and composite models

We further investigated the possibility that a steep ($\Gamma = 1.9$) power law passing through a warm absorber can give an apparently flat 0.4-10 keV spectrum. In contrast to a neutral absorber (where we use a partial covering model), this model interprets absorption as being due to highly ionized gas that completely covers the continuum source. The presence of absorption due to ionized matter has currently been confirmed in several Seyfert 1 galaxies (see Matsuoka 1994 for a review) and may also contribute significantly to the soft X-ray emission of intermediate Seyfert galaxies such as NGC4151 (Weaver et al. 1994b). We therefore investigated whether a warm absorber can explain both the soft excess and flat spectrum of NGC5252.

A simple model of a warm absorber using the “CLOUDY” photoionization code (Ferland 1991) has been constructed. Following Fabian et al. (1994), we assumed that a shell of gas with solar abundances, density $10^8 - 10^{10} \text{ cm}^{-3}$, and uniform temperature is uniformly distributed around an ionizing power law continuum source with $\Gamma = 1.9$ and luminosity $L = 10^{43} \text{ erg s}^{-1}$. The emergent spectrum, consisting of the transmitted continuum plus the emission from the shell, was fitted to the SIS data. The free parameters were the “warm” column density N_W (cm^{-2}), the ionization parameter $\xi = L/nR^2$ ($\text{erg s}^{-1} \text{ cm}$) and the normalization constant of the warm absorber model. The model gave a poor fit to the data (with $\chi_{red}^2/d.o.f. = 1.32/314$) and strong systematic differences between the model and the data were evident between 0.7 and 1.6 keV. Indeed, the warm absorber hypothesis does not work unless another soft component is added because the strong edges around 1 keV predicted by the model (Netzer 1993, Krolik & Kriss 1995) are not seen in the data.

We then repeated the fitting procedure with an additional power law to model a soft scattered component (increasing the number of free parameters to 5). The photon index of the warm absorbed power law was again fixed to 1.9 but that of the scattered component was free to vary. All other parameters were also varying. The resulting

composite scattering + warm absorber model yielded an acceptable fit with $\chi_{red}^2/d.o.f. \simeq 0.96/311$. The best-fit model is shown in Figure 5 and the interesting best-fit parameters are $\log N_W \simeq 22.88 \pm 0.02$, $\log \xi \simeq 1.61 \pm 0.04$ and $\Gamma \simeq 1.43_{-0.73}^{+0.41}$ for the scattered component. For two interesting parameters, the 90% upper limit for the photon index of the scattered component is ~ 1.92 .

Thus, when the spectrum of NGC5252 is modelled with a composite warm absorber plus (scattered) power law, an intrinsic index as steep as 1.92 cannot be ruled out. However, despite the higher number of free parameters, the statistics are worse than with the single partial covering model, probably because of the presence of systematic positive residuals at high ($E > 6$ keV) energies (Figure 5).

3.3.3 Composite “dual-absorber” model

A further possibility to mask a steep intrinsic continuum slope is through the presence of an additional, strongly absorbed power law. This could considerably flatten the observed spectrum in the ASCA energy band, similar to a very strong reflection component. We then fitted the data by adding a second absorbed power law to the partial covering model. The resulting spectral model can be interpreted as a single power law undergoing absorption by material with 2 different column densities that partly, but not completely, cover the source. For example, this may be a crude approximation of a nonuniform density distribution of clouds along the line of sight.

The resulting composite “dual-absorber” model is of the form: partial covering absorption \times power law (1) + partial covering absorption \times power law (2). Photon indices and covering fractions were fixed to be equal for both components, leading to a total of 6 free parameters, namely the 2 different absorptions (N_{H1} and N_{H2}), the 2 normalizations $A(1)$ and $A(2)$, the covering fraction C_F , and the photon index.

The model yielded an acceptable description of the source spectrum with $\chi_{red}^2/d.o.f. \simeq 0.92/311$. The resulting best-fit parameters reported in Table 7 are consistent with an intrinsically steep ($\simeq 1.86 \pm 0.3$) power law source almost completely ($\sim 98\%$) covered by two distinct absorption columns with $\sim 4.8 \times 10^{22}$ cm $^{-2}$ (for $\sim 55\%$ of the covering matter) and $\sim 6.2 \times 10^{23}$ cm $^{-2}$ (for $\sim 45\%$ of the covering matter). As is evident from the best-fit model shown in Figure 6a, the strongly absorbed power law could well flatten

the hard part of the spectrum in the ASCA energy band. Therefore, this model provides a viable description of the spectrum of NGC5252 consistent with a steep power law. It will be considered again in section 4.2.

The results obtained with the scattering model are also shown for comparison in Figure 6b. As stated above, the fits are algebraically equivalent, but in the scattering case the spectral model could be related to a physical scenario where the continuum is (completely) covered by a torus of nonuniform density, whereas part of the continuum emission is scattered into the line of sight by highly ionized matter present in the vicinity of the nucleus.

3.4 Iron emission line

We inspected the SIS spectra for the presence of an iron emission line feature and our results are summarized in Table 8.

With the continuum described by a thermal component plus an absorbed power law ($\Gamma \sim 1.2$), as given in section 3.2.1, we obtain an upper limit for the equivalent width of an iron $K\alpha$ line of $EW \lesssim 120$ eV. With the single partial covering model ($\Gamma \sim 1.45$, section 3.2.2), though the feature is only marginally visible in the data (Figure 2), a narrow emission line is detected. The inclusion of a narrow line at the fixed energy $E=6.254$ keV improves the fit to more than 99.5 % confidence level ($\Delta\chi^2 \simeq 8$ for 311 d.o.f.). With the energy of the line free to vary, the best-fit value found is $EW \simeq 90_{-49}^{+63}$ eV when the width is fixed to 0, and $EW \simeq 100_{-59}^{+62}$ eV when the width is free, with $\sigma \lesssim 118$ eV (Table 8). These results agree with the emission of a fluorescent narrow Fe $K\alpha$ line from matter in a neutral state (Makishima 1986).

With the continuum modelled by a partial covering plus reflection component, the line becomes slightly weaker, with $EW \simeq 78_{-53}^{+44}$ eV. This value is of particular interest because it can be directly compared with the expected EW from the reflection component, as shown in section 4.2.

The line is remarkably weak when compared to reported values for other Seyfert 2 galaxies (e.g., Kunieda et al. 1994). As far as results from the iron line diagnostics are concerned, there is no need for “complex” geometries in the case of NGC5252. A simple line-of-sight absorber, uniformly distributed around the source, can explain the

observed iron line intensity of NGC5252 (Makishima 1986, Leahy & Creighton 1993). We emphasize that no absorption edge, expected from neutral matter, has been detected at the redshifted energy of $E = 6.94$ keV. The upper limit derived is $\tau \lesssim 0.16$ at a 90% confidence level. At higher energies there is no evidence for a Fe K edge produced by ionized matter, either.

4 Discussion

4.1 Soft excess

We have shown that the observed strong soft excess in NGC5252 can well be described by either a scattering model or a partial covering model. Thermal models are unlikely.

Recent ASCA observations clearly detected thermal emission associated with starburst activity from the stereotype Seyfert 2 galaxy NGC1068 (Ueno et al. 1994). A similar component is unlikely in the case of NGC5252; its host galaxy is an early-type galaxy which doesn't exhibit strong stellar activity. More specifically, given a far-infrared luminosity of $\sim 6 \times 10^9 L_{\odot}$, the fitted soft X-ray luminosity of $L_x(0.4-2 \text{ keV}) \sim 6 \times 10^{41} \text{ erg cm}^{-2} \text{ s}^{-1}$ exceeds the value expected from the far-infrared/X-ray luminosity correlation for bright infrared normal and starburst galaxies (David, Jones & Forman 1992) by approximately 2 orders of magnitude. This strongly suggests that the AGN inside NGC5252 is directly responsible for the observed soft excess and excludes strong stellar activity (e.g., X-ray binaries and Supernovae Remnants) associated with the host galaxy. Moreover, a hot thin collisionally ionized plasma at a temperature of $T \sim 9 \times 10^6$ K should produce a blend of emission lines (mostly from Fe L) in the energy range 0.8 to 1.2 keV, which are not detected (section 3.2.1). A one-temperature thermal plasma is therefore ruled out by the data, unless the metal abundances are very small ($\lesssim 0.01$ solar).

As long as the scattering zone is not highly ionized ($T \sim 10^5$ K), the scattering model predicts the presence of oxygen absorption edges between 530 and 870 eV, depending on the ionization state. An estimate of the expected oxygen optical depth τ_o due to the scattering material is given by $\tau_o \sim A_o f_{scatt} \sigma_o (\sigma_e c_f \times \Omega/4\pi)^{-1}$ (Weaver et al. 1994a), where A_o , f_{scatt} , σ_o , σ_e , c_f and $\Omega/4\pi$ are the oxygen abundance, the fraction of scattered

flux, the oxygen and electron scattering cross sections, the covering fraction, and the solid angle of the scattering matter, respectively. From the measured opening angle of $\sim 75^\circ$ for the ionization cones and the best-fit value $f_{scatt} \sim 0.04$, assuming $c_f = 1$ for the scattering medium and cosmic abundances, we estimate a value of $\tau_o \sim 11$. However, there is no evidence for such a strong edge in our data. As an example, the upper limit we measure for the OVIII edge at 0.85 keV (the strongest at soft energies) is $\tau \lesssim 1.5$. These results make the presence of a $T \sim 10^5$ K scattering matter in NGC5252 unlikely.

If the scattering region is highly ionized, X-rays are efficiently scattered and no absorption features are expected. Soft (~ 900 eV) emission lines, typically with EW $\lesssim 100$ eV, are instead expected for a highly photoionized gas (Netzer 1993). In the case of NGC5252, the data do not allow significant detection of any soft X-ray feature, but cannot rule out soft emission lines of up to several hundreds eV, either. The existence of a hot ($T \sim \text{few} \times 10^6$ K) gas has been postulated by Marshall et al. (1993) to explain the higher ionization states indicated by multiple Fe K and Fe L emission lines observed in the BBXRT spectrum of NGC1068. Also in the case of NGC5252, gas inside its bicone might be highly photoionized since it directly sees the nuclear source and, therefore, could scatter the X-ray continuum into our line of sight producing the observed soft excess. Polarization of the optical-UV continuum light should then be detected along the ionizing bicone. The recent blue (3200-6200 Å) spectropolarimetric observations conducted by Kay (1994) are, however, not very encouraging as no clear polarization was detected ($P \simeq 11\% \pm 11\%$). As proposed by the author, imaging polarimetry or spectropolarimetry with the slit aligned along the axis of the cone could be more fruitful.

On the other hand, the partial covering model (Holt et al. 1980) doesn't predict any soft X-ray line emission as the observed soft radiation escapes directly from the source. Since no X-ray variability was detected with ASCA, it is impossible to distinguish between a partial covering and scattering model with the present data. High spatial resolution X-ray observations with the HRI onboard ROSAT could easily resolve some extended emission (if present), or/and optical-UV polarimetric observations could help to discriminate between these two models.

4.2 The flat spectrum problem

The flat spectrum **and** weak iron line differentiates NGC5252 from the majority of known Seyfert 2 galaxies. X-ray spectra of most Seyfert 1 galaxies are found to be consistent with a steep intrinsic spectrum ($\Gamma_{2-18keV} \sim 1.8 - 2.1$, when reflection is accounted for) and relatively strong ($EW \sim 120 - 160$ eV) fluorescent iron lines (e.g., Nandra & Pounds 1994). GINGA observations of Seyfert 2 galaxies (Awaki et al. 1991) and recent ASCA observations (e.g., NGC6552: Fukazawa et al. 1994; NGC1068: Ueno et al. 1994) indicate that several Seyfert 2 galaxies have a flat hard X-ray spectrum and a strong ($EW \sim$ several hundred eV) fluorescence iron line (Kunieda et al. 1994).

These features (flat spectrum and strong iron line), first detected by GINGA and now confirmed by ASCA, are often interpreted as the signature of reflection of radiation from cold matter (e.g., Reynolds et al. 1994). In the case of NGC5252, results from section 3.3.1 show that the data require a very strong ($R \sim 7$) reflection component to explain the observed flat spectrum. This high amount of reflection, if true, implies an anisotropic radiation field, i.e. the reflector “sees” more radiation than is observed directly (Ghisellini et al. 1991), or/and that there is a time lag effect. However, we believe that a substantial contribution from a reflection component is unlikely because it predicts a stronger iron line than observed. In fact, assuming cosmic abundances, the equivalent width (EW_{refl}) of the iron line relative to the reflection component (measured at the line energy) is of the order of ~ 1 keV. We obtained this result from performing Monte Carlo simulations in the simplest case of a slab geometry (Lightmann & White 1988), but as a rough estimate it holds for almost all geometries and for a wide range of column densities (10^{22} to 10^{24} cm $^{-2}$) of the reflecting matter (see Makishima 1986 and Awaki et al. 1991 for calculations with spherical and toroidal geometries, respectively). With the relationship $EW_{refl} \sim 1$ keV, the best-fit reflection model predicts an equivalent width (calculated with respect to the power law plus reflection continuum) of $\simeq 400 \pm 250$ eV for the iron line. This value is about 5 times larger than the value ($EW \simeq 78 \pm 50$, section 3.4) measured from the data. One should point out that the two values are still consistent within 90% confidence (for two interesting parameters) because of the large errors associated with the parameters of the reflection component, but they exclude each other at the 1σ level. The lack of a strong iron line in NGC5252

suggests that a strong contribution from a reflection component, as possible explanation of the flat spectrum, is unlikely.

One possible objection to the above comes from the edge-on geometry of NGC5252, as inferred from optical observations discussed in section 1. Our previous assumption of a slab observed face-on (the inclination was fixed to 0 in section 3.3.1) may not be correct and a larger inclination angle might have been more natural. However, the effect of a higher inclination would be to diminish the “efficiency” of the reflection. This effect would therefore be compensated in the fitting procedure by an increase of the normalization of the reflection component, leaving the above conclusions unchanged. It could also be argued that a different geometry for the reflector, like that of a (neutral) broad line region (Yaqoob et al. 1993a, Nandra & George 1994) or a molecular torus (Ghisellini, Haardt & Matt 1994, Krolik et al. 1994) may provide an alternative description for the observed spectral flatness. However, in all cases we would have to face the problem of the absence of a strong iron line.

Of course if the Fe abundances are reduced the value of the EW can be made to match the observed one. However we do not regard this as a realistic possibility as observational evidence indicates that, at least for some Seyfert 2 galaxies, the tendency is to have Fe overabundances. Another alternative possibility comes from theoretical arguments. Ross & Fabian (1993) and Zycki & Czerny (1994) showed that for a range of ionization stage of iron ions within $15 \lesssim \langle Fe \rangle \lesssim 22$, or if iron is fully ionized, the Fe line EW can be very low even in the presence of strong reflection. However, it should be emphasized that the presence of highly ionized material is compatible only with the case of reflection from an accretion disk or, possibly, from a broad line region (Netzer 1993), but not from a torus. Moreover, in the case of ionized reflection, the substantial lack of photoelectric absorption yields a slope of the reflection component which is typically the same (or even steeper) than that of the intrinsic power law. The Fe K line center energy is also expected at slightly higher energies than observed if the gas is ionized. Therefore, the use of ionized reflection instead of neutral reflection wouldn't be justified in this case.

We also found that a dual-absorber model (section 3.3.3) could explain the observed flat spectrum with an intrinsically steep power law ($\Gamma \simeq 1.86 \pm 0.3$). The deduced

spectral shape (Figures 6a or 6b) is very similar to that expected with a reflection component (Figure 4) but in this case, a strong emission line is not expected a priori. The only constrain could come from the absorption edge at the redshifted energy of 6.94 keV, as expected by neutral absorption. The model predicts an absorption edge with optical depth $\tau \simeq 0.21_{-0.11}^{+0.68}$ which is consistent with the measured upper limit of $\tau \lesssim 0.16$ (see section 3.4). Therefore, nonuniform cold absorption provides an adequate explanation for the observed flat spectrum of NGC5252. The absorbing material may be interpreted as a distribution of clouds with nonuniform density, e.g. with higher densities at smaller radii. Alternatively, it may consist of an absorbing torus with nonuniform density. In this case, since the absorption is $\sim 10^{22-23} \text{ cm}^{-2}$, while predicted columns of absorption tori are $\sim 10^{24-25} \text{ cm}^{-2}$, either (1) the torus is intrinsically optically thin or (2) we are looking through its rim.

Another possible interpretation for the flat spectrum of NGC5252 is that it is intrinsically flat. In a re-analysis of GINGA data, Smith and Done (1995) found several other Seyfert 2 galaxies with flat power law spectra similar to that observed in NGC5252, but with slightly higher iron line EW $\sim 100 - 150 \text{ eV}$. These authors also found that at least 4 of the sources are incompatible with a steep slope, even with the inclusion of a reflection component. A recent analysis of combined GINGA and OSSE data by Zdziarski et al. (1994) indicate that the intrinsic X-ray spectra of some Seyfert 2 galaxies may be substantially harder than those of Seyfert 1s, in contrast to unified models of AGN. Their slopes are consistent with our results for NGC5252.

Finally, we would like to comment on the strong resemblance between the ASCA X-ray spectrum of NGC5252 and the BBXRT and ASCA spectra of NGC4151 (Weaver et al. 1994a, Weaver et al. 1994b). Both sources reveal a strong ($L_X(0.1-2.0) \sim 10^{41} \text{ erg s}^{-1}$) soft excess below $\sim 2 \text{ keV}$, an absorption around $10^{22-23} \text{ cm}^{-2}$, a flat continuum ($\Gamma \sim 1.3 - 1.7$), a high ($\gtrsim 0.90$) covering fraction and a relatively weak iron line ($\sim 50 - 150 \text{ eV}$) (Yaqoob et al. 1993b, Weaver et al. 1994b). Both objects are relatively low luminosity Seyfert galaxies with $L_X(2-10 \text{ keV}) \sim 2 \times 10^{43} \text{ erg s}^{-1}$ (NGC5252) and $L_X(2-10 \text{ keV}) \sim 10^{43} \text{ erg s}^{-1}$ (NGC4151; Seyfert 1.5). These strong similarities suggest that the hard spectrum of NGC5252 may be intrinsically flat, as seems to be the case for NGC4151.

A better understanding of these Seyfert galaxies with flat spectra is of fundamental importance, not only because the problem has direct implications for unified models, but also because they could help explaining the so-called “spectral paradox” (Boldt 1987), i.e. the difference between the X-ray spectra of AGN and that of the CXB.

5 Conclusion

The analysis of the X-ray spectrum of NGC5252 shows that a single absorbed power law alone can describe the 0.7-10 keV GIS spectrum but there is evidence of a strong soft excess in the 0.4-10 keV SIS spectrum. We argue against a thermal origin of the soft excess because there is no indication of starburst activity in NGC5252 and we do not observe the expected soft emission lines produced by a plasma at $T \sim 10^6$ K.

The best description for the 0.4-10 keV spectrum is provided by a partial covering model or a scattering model, both models being equally compatible with the current data. The main results of the spectral analysis are a very flat ($\Gamma \simeq 1.45 \pm 0.23$) power law, a high covering fraction ($C_f \simeq 0.96 \pm 0.01$) from thick ($N_H \simeq 4.3 \pm 0.6 \times 10^{22} \text{ cm}^{-2}$) material and a weak ($EW \simeq 90 \pm 60 \text{ eV}$) iron line. The scattering model gives the same best-fit parameters, with a fraction $\sim 4\%$ of scattered light.

The flat spectral shape is incompatible with current theories of Seyfert unification schemes which predict steeper intrinsic power laws of $\Gamma \sim 1.8 - 2.1$. The flat slope **and** weak Fe K iron line measured in NGC5252 make the reflection hypothesis unlikely, but it cannot be ruled out. The inclusion of a warm absorber, instead of a neutral absorber to explain the flat spectrum gives systematic deviations at higher energies yielding a fit statistically worse than with only partial covering. A complex partial covering model with two different column densities (composite dual-absorber model) with a canonical steep ($\Gamma \sim 1.9$) power law offers a potential explanation for the flatness of the spectrum. An alternative interpretation of the present data is that the measured X-ray spectrum of NGC5252 is intrinsically flat.

6 Acknowledgements

The authors wish to thank the referee, Kim Weaver, for helpful and constructive comments, all the ASCA team members for making this observation possible and K. Leighly for a careful reading of the manuscript. M.C. thanks A. Comastri, S. Molendi, Y. Ogasaka, S. Ueno and T. Yamada for helpful discussions. M.C. also acknowledges financial support from the Science and Technology Agency of Japan (STA fellowship), hospitality from the RIKEN Institute and support from the European Union. G.G.C.P. acknowledges partial financial support from MURST and ASI.

7 References

- Antonucci, R.R.J., 1993, *ARA&A*, 31, 473
- Antonucci, R.R.J. & Miller, J.S., 1985, *ApJ*, 297, 621
- Arnaud, K.A. et al., 1991, *XSPEC User's Guide*, ESA TM-09
- Avni, Y., 1976, *ApJ*, 210, 642
- Awaki, H. et al., 1991, *PASJ*, 43, 195
- Boldt, E. 1987, *Phys. Repts.*, 146, 215
- David, L.P., Jones, C. & Forman, W., 1992, *ApJ*, 388, 82
- Dickey, J.M. & Lockman, F.J., 1990, *ARA&A*, 28, 215
- Fabian, A.C. et al., 1994, *PASJ*, 46, L59
- Ferland, G.J., 1991, OSU Internal report, N. 91-01
- Fukazawa, Y. et al., 1994, *PASJ*, 46, L141
- George, I.M. & Fabian, A.C., 1991, *MNRAS*, 249, 352
- Ghisellini, G., et al., 1991, *MNRAS*, 248, 14
- Ghisellini, G., Haardt, F. & Matt, G., 1994, *MNRAS*, 267, 743
- Guilbert, P.W., & Rees, M.J., 1988, *MNRAS*, 233, 475
- Holt, S.S. et al., 1980, *ApJ*, 241, L13
- Kay, L., 1994, *ApJ*, 430, 196
- Krolik, J.H., Madau, P. & Zycki, P.T., 1994, *ApJ*, 420, L57
- Kotilainen, J. & Prieto, M.A., 1994, *A&A*, 295, 649
- Koyama, K. et al., 1989, *PASJ*, 41, 731
- Krolik, J.H. & Kriss, G.A., 1995, preprint.
- Kunieda, H. et al. 1994, in “New Horizon of X-ray Astronomy”, ed. F. Makino & T. Ohashi, (Tokyo: Universal Academy Press), p317
- Lampton, M., Margon, B. & Bowyer, S., 1976, *ApJ*, 208, 177
- Leahy, D.A. & Creighton, J., 1993, *MNRAS*, 263, 314
- Lightman, A.P. & White, T.R., 1988, *ApJ*, 335, 57
- Makishima, K. 1986, *Lecture Notes in Physics*, 266, 249
- Marshall, F.E. et al., 1993, *ApJ*, 405, 168
- Matsuoka, M. 1994, in “New Horizon of X-ray Astronomy”, ed. F. Makino & T. Ohashi, (Tokyo: Universal Academy Press), p305

Miller, J.S. & Goodrich, R.W., 1990, ApJ, 355, 456
Morrison, R. & McCammon, D., 1983, ApJ, 270, 119
Nandra, K. & George, I.M., 1994, MNRAS, 267, 974
Nandra, K. & Pounds, K.A., 1994, MNRAS, 268, 405
Netzer, H., 1993, ApJ, 411, 594
Otani, C. & Dotani, T., 1994, Asca News n.2, 25
Prieto, M.A. & Freudling, W., 1993, ApJ, 418, 668
Prieto, M.A. & Freudling, W., 1995, MNRAS, submitted
Raymond, J.C. & Smith, B.W., 1977, ApJS, 35, 419
Reynolds, C.S. et al., 1994, MNRAS, 268, L55
Ross, R.R. & Fabian, A.C., 1993, MNRAS, 261, 74
Ruiz, M., Rieke, G. & Schmidt, G., 1994, ApJ, 423, 608
Smith, D.A., & Done, C., 1995, submitted to MNRAS
Tadhunter, C. & Tsvetanov, Z., 1989, Nature, 341, 422
Tran, H.D., Miller, J.S. & Kay, L.E., 1992, ApJ, 397, 452
Ueno, S. et al., 1994, PASJ, 46, L71
Unger, S.W. et al, 1987, MNRAS, 228, 671
Weaver, K.A., Arnaud, K.A. & Mushotzky, R.F., 1995, ApJ, in press
Weaver, K.A. et al., 1994a, ApJ, 423, 621
Weaver, K.A. et al., 1994b, ApJ, 436, L27
Wilson, A.S. & Tsvetanov, Z.I., 1994, A.J., 107, 1227
Yaqoob, T. et al., 1993a, ApJ, 416, L5
Yaqoob, T. et al., 1993b, MNRAS, 262, L435
Zdziarski, A.A. et al., 1994, ApJL, 438, L63
Zycki, P.T. & Czerny, B., 1994, MNRAS, 266, 653

Table 1 : Selection criteria

GIS	SIS
SAA=0	SAA=0
COR_MIN > 7	COR_MIN > 6
ELV_MIN > 5	ELV_MIN > 5
–	BR_EARTH > 25
–	T_DY_NT > 100

SAA: South Atlantic Anomaly

COR_MIN: Cut-off rigidity (GeV/c)

ELV_MIN: Minimum elevation angle from earth (degree)

BR_EARTH: Minimum bright earth angle (degree)

T_DY_NT: Time after a day/night transition (s)

Table 2 : Exposure times and count rates

	exposure (s)	Source + Backg. (counts)	Backg. (counts/s)	Source (counts/s)
GIS2	70970	4011	0.011	0.045
GIS3	70747	5194	0.012	0.061
SIS0	65154	4235	0.010	0.055
SIS1	64448	3736	0.008	0.050

Table 3: GIS and SIS - Single Power Law

	N_{H} (10^{22} cm^{-2})	Γ	$F_{\text{X}}^a(0.7-10 \text{ keV})$ ($10^{-12} \text{ erg cm}^{-2} \text{ s}^{-1}$)	$\chi_{\text{red}}^2/\text{d.o.f.}$
GIS2	$3.76^{+0.84}_{-0.75}$	$1.35^{+0.25}_{-0.24}$	8.23	0.83/118
GIS3	$3.91^{+0.71}_{-0.63}$	$1.43^{+0.20}_{-0.20}$	9.77	0.99/146
BOTH	$3.83^{+0.54}_{-0.49}$	$1.39^{+0.16}_{-0.15}$	9.00	1.03/267
SIS0	$2.13^{+0.73}_{-0.52}$	$0.84^{+0.31}_{-0.24}$	9.00	1.39/165
SIS1	$2.52^{+0.73}_{-0.52}$	$1.05^{+0.32}_{-0.30}$	9.46	1.36/145
BOTH	$2.34^{+0.48}_{-0.44}$	$0.95^{+0.20}_{-0.20}$	9.20	1.38/313

^a corrected for absorption.

Note: Intervals are at 90 % confidence for 2 interesting parameters.

Table 4: SIS – Two component models

	Ab.	kT (keV)	N_{H} (10^{22} cm $^{-2}$)	Γ	L_{X}^a (0.1-2.0 keV) (10^{41} erg s $^{-1}$)	$\chi_{red}^2/\text{d.o.f.}$
black body + abs(PL)	...	$0.18_{-0.03}^{+0.05}$	$3.04_{-0.53}^{+0.74}$	$1.17_{-0.16}^{+0.20}$	3.86	0.94/311
bremss. + abs(PL)	...	$0.80_{-0.33}^{+1.23}$	$3.45_{-0.62}^{+0.83}$	$1.26_{-0.24}^{+0.26}$	6.47	0.93/311
R-S ^b + abs(PL)	< 0.01	$0.77_{-0.24}^{+1.18}$	$3.46_{-0.66}^{+0.84}$	$1.26_{-0.18}^{+0.23}$	6.44	0.92/310

^a calculated with only the soft component.

^b R-S = Raymond-Smith (with abundances Ab).

Note: Intervals are at 90 % confidence for 3 interesting parameters.

Table 5a: SIS – Partial covering model

N_{H}	C_F	Γ	$F_{\text{x}}^a(0.4-10 \text{ keV})$	$\chi_{\text{red}}^2/d.o.f.$
$(10^{22} \text{ cm}^{-2})$			$(10^{-12} \text{ erg cm}^{-2} \text{ s}^{-1})$	
$4.33_{-0.61}^{+0.66}$	$0.96_{-0.02}^{+0.01}$	$1.45_{-0.23}^{+0.23}$	11.69	0.95/312

Table 5b: SIS – Scattering model

N_{H}	$A(1)/A(2)^b$	Γ	$F_{\text{x}}^a(0.4-10 \text{ keV})$	$\chi_{\text{red}}^2/d.o.f.$
$(10^{22} \text{ cm}^{-2})$			$(10^{-12} \text{ erg cm}^{-2} \text{ s}^{-1})$	
$4.39_{-0.64}^{+0.68}$	0.046	$1.46_{-0.23}^{+0.23}$	11.69	0.95/312

^a corrected for absorption.

^b $A(1)/A(2) = \frac{\text{normalization of the scattered component at 1 keV}}{\text{normalization of the continuum at 1 keV}}$

Note: Intervals are at 90 % confidence for 3 interesting parameters.

Table 6: SIS – Partial covering + reflection

N_{H}	C_F	A_{pl}^a	A_{reff}^a	Γ_{int}	$\chi_{\text{red}}^2/d.o.f.$
(10^{22} cm^{-2})					
$4.61_{-0.39}^{+0.40}$	$0.97_{-0.01}^{+0.01}$	2.19	$15.6_{-12.3}^{+16.3}$	$1.91_{-0.33}^{+0.33}$	0.92/311

^a normalization at 1 keV in units of $10^{-3} \text{ photons cm}^{-2} \text{ s}^{-1} \text{ keV}^{-1}$.

Note: Intervals are at 90 % confidence for 1 interesting parameter.

Table 7: SIS – Composite dual-absorber model

N_{H1}	$A^a(1)$	C_F	Γ	N_{H2}	$A^a(2)$	$\chi^2_{red}/d.o.f.$
(10^{22} cm^{-2})				(10^{22} cm^{-2})		
$4.82^{+0.40}_{-0.37}$	2.17	$0.98^{+0.01}_{-0.01}$	$1.86^{+0.26}_{-0.31}$	62^{+64}_{-25}	1.75	0.92/311

^a normalization at 1 keV in units of $10^{-3} \text{ photons cm}^{-2} \text{ s}^{-1} \text{ keV}^{-1}$.

Note: Intervals are at 90 % confidence for 1 interesting parameter.

Table 8: SIS – Fe K line best-fit parameters

Continuum model	E (keV)	σ (eV)	EW (eV)
Raymond-Smith + Power law	$6.25^{+0.05}_{-0.16}$	0 (fixed)	$\lesssim 120$
Partial covering	$6.25^{+0.05}_{-0.07}$	0 (fixed)	90^{+63}_{-49}
	$6.25^{+0.05}_{-0.03}$	$\lesssim 118$	100^{+62}_{-59}
Partial covering + Reflection	$6.24^{+0.07}_{-0.08}$	0 (fixed)	78^{+44}_{-53}

Note: Intervals are at 90 % confidence for 1 interesting parameter.

Figure captions

Figure 1: SIS spectrum and associated residuals obtained from the simultaneous joint fit of SIS0 and SIS1 instrument data with a single absorbed power law. The solid line represents the best-fit power law modelled to the spectrum between 0.4 - 10 keV. A soft excess below 1.2 keV is clearly evident.

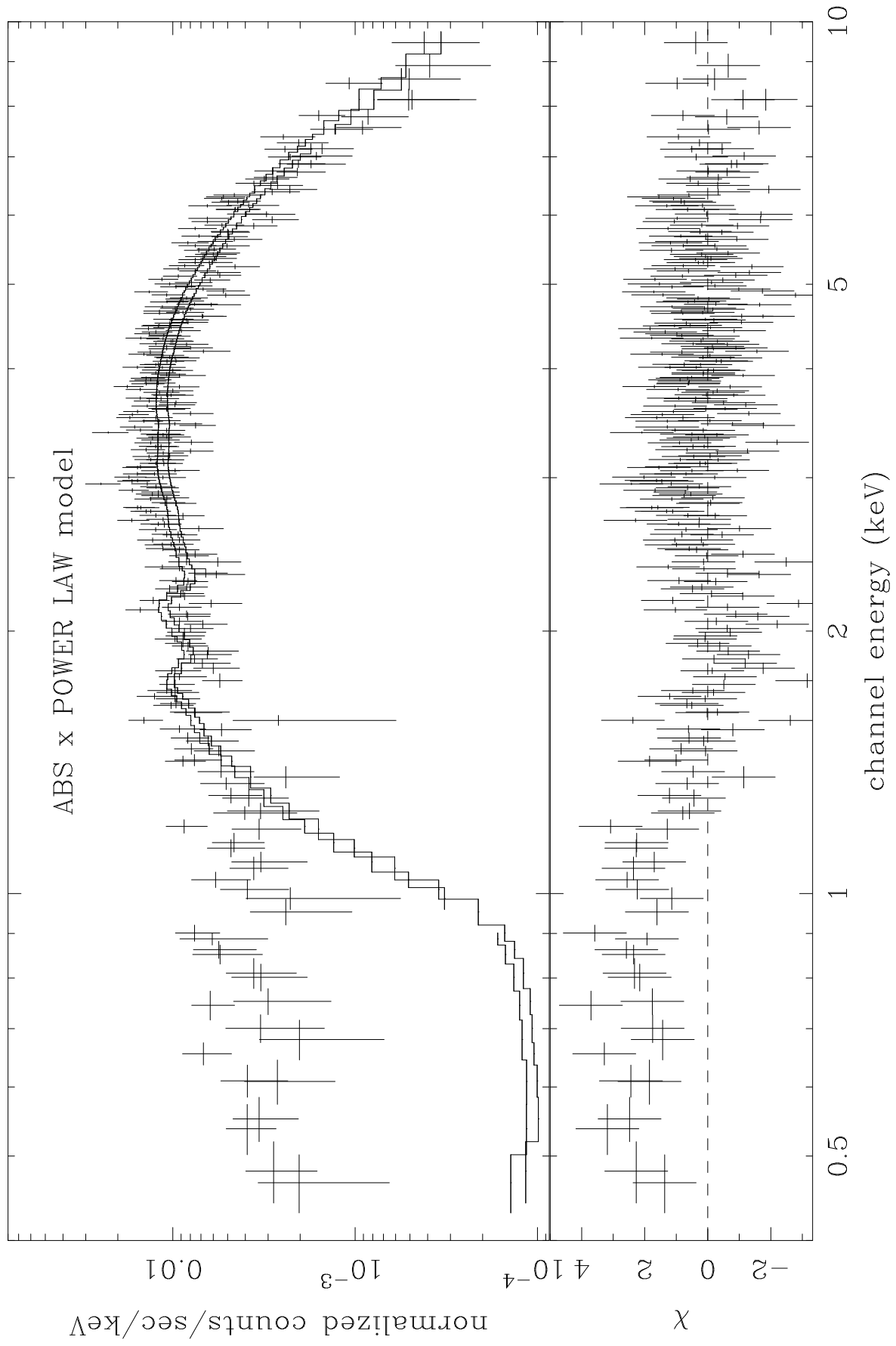
Figure 2: Unfolded SIS spectrum with the partial covering model. The solid line represents the best-fit partial covering model.

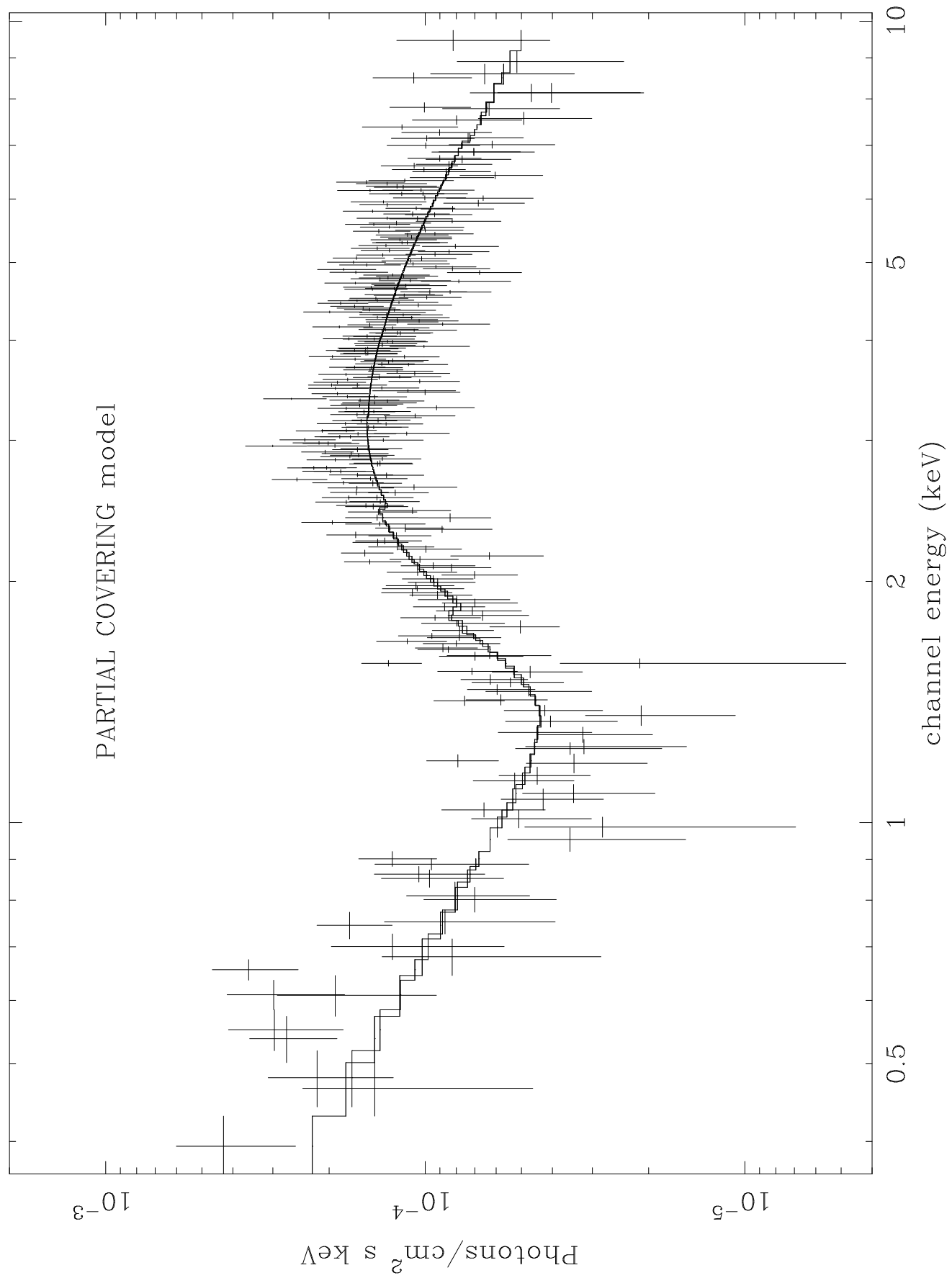
Figure 3: Confidence contours for photon index vs column density (*top*) and covering fraction vs column density (*bottom*) for the best fit obtained with the partial covering model. Contours are at 68%, 90% and 99% confidence levels.

Figure 4: SIS best-fit model and associated residuals with the partial covering + reflection component model.

Figure 5: SIS best-fit model and associated residuals with the scattering + warm absorber model.

Figure 6: (a) SIS best-fit model and associated residuals with the partial covering + “dual-absorber” model. (b) SIS best-fit model and associated residuals with the scattering + “dual-absorber” model.





Confidence contours – partial covering model

